The influence of siliciclastic content on the strength and deformation behavior of rock salt – Constraints from thermomechanical experiments

5   Jolien Linckens[1,2], Mareike Henneberg[3,4], Janet Zulauf[1], Elke Hattingen[5], Michael Mertineit[3], Gernold Zulauf[1]

[1] Institut für Geowissenschaften, Goethe-Universität Frankfurt a.M., Altenhöferallee 1, D-60438 Frankfurt a.M., Germany
[2] Now at: Tata Steel, R&D, Microstructural and Surface Characterisation, P.O. Box 10.000, 1970 CA Ijmuiden, The
10 Netherlands
[3] Bundesanstalt für Geowissenschaften und Rohstoffe (BGR), Stilleweg 2, 30655 Hannover, Germany
[4] Now at: CSD Ingenieure AG, Schachenallee 29A, 5000 Aarau, Switzerland
[5] Institut für Neuroradiologie, Universitätsklinikum, Goethe-Universität, Schleusenweg 2-15, D-60528 Frankfurt a.M., Germany.

15 *Correspondence to*: Jolien Linckens (jolienlinckens@gmail.com)

Abstract. Halite forms the main constituent of rock salt, which is regarded as a possible host rock for nuclear waste repositories and storage caverns. The deformation behavior of pure halite and rock salt has been revealed by microfabric analyses of naturally and experimentally deformed samples. Such studies, however, are rare for rock salt with significant amount of secondary phases (e.g., siliciclastics, clay, anhydrite), although these are also common in nature. In order to determine the

20 influence of siliciclastic material on the deformation behaviour of rock salt, we performed deformation experiments using rock salt samples with variable siliciclastic content (1, 7, 38 and 53 vol. %). The experiments were conducted under bulk flattening strain, elevated temperature (345°C), low differential stress (<4.6 MPa), and a strain rate of 10-7 s-1. To gain inside in the 3D distribution of the siliciclastic material and in the deformation mechanisms of the constituent minerals, computer tomographic (CT), microstructural and electron backscatter diffraction (EBSD) analyses were applied to both initial and experimentally

25 deformed samples. The EBSD and microstructural data suggest that, independent of the amount of siliciclastic content, the deformation of the halite matrix was largely accommodated by subgrain formation without subgrain rotation recrystallization. The deformation of the siliciclastic domains, on the other hand, was entirely brittle. CT images show open fractures, oriented sub-perpendicular to the least principal stress, $\sigma 3$. An increase in the siliciclastic content leads to an increase in differential stress of the halite matrix. The new results suggest that the barrier properties of rock salt is significantly reduced by larger

30 content of siliciclastic material, particularly in cases where the siliciclastic parts and their fractures are interconnected making pervasive ascendant fluid transport possible in these lithological units. Future thermomechanical experiments of impure rock salt should focus on the effect of confining pressure, which is expected to reduce the number and width of open fractures in the siliciclastic domains.

1 Introduction

35 Rock salt is composed mainly of the mineral halite (Hudec and Jackson, 2007) and flows at low temperatures (25°C) and small differential stresses (<2 MPa) (e.g., Urai et al., 2008). Due to the low density and viscosity of rock salt, it can form pillows and diapirs. Salt diapirs are important structures, as they can function as petroleum traps. Low porosity and viscosity, combined with high thermal conductivity, makes rock salt a potential host rock for the deep geological repository of nuclear waste (e.g., von Berlepsch & Haverkamp, 2016; Bornemann et al., 2008). In addition, salt caverns are used as storage site of hydrocarbons

40 for energy supply (e.g., Staudtmeister & Rokahr, 1997).

The deformation behavior of halite has been studied in great detail. This holds for both natural and experimentally deformed samples. Deformation experiments indicate that dislocation creep (e.g., Carter & Hansen, 1983; Franssen, 1994; Linckens et al., 2016; Peach et al., 2001; Skrotzki et al., 1996) and pressure-solution creep (e.g., Spiers et al., 1990; Spiers & Urai, 2007; Urai, Spiers, et al., 1986) are the dominant ductile deformation mechanisms in rock salt. A prerequisite for the occurrence of

45 pressure solution is the presence of a thin fluid film on the halite grain boundaries (Spiers et al., 1990). Studies on natural rock salt shows that often fluid inclusions occur on the grain boundaries of halite (e.g., Urai et al., 1986; Küster et al., 2008; Desbois et al., 2012; Kneuker et al., 2014). Pressure solution works particularly well if wet rock salt is deformed in an open system, such as salt glaciers, but is less common in dry and coarse-grained (cm-scale) wet rock salt (e.g., Urai et al., 2008) and in salt rocks, which act as a closed system. In such closed systems, the saturated fluid cannot escape from, and the undersaturated

50 fluid cannot enter into the deforming salt rock. This explains the lack of stylolites and other solution phenomena in rock salt situated at deeper structural levels, where dislocation creep is the dominant deformation mechanism. During dislocation creep, recovery by grain boundary migration (GBM) and subgrain formation take place in naturally and experimentally deformed rock salt (e.g., Desbois et al., 2010; Franssen, 1994; Ter Heege et al., 2005). The subgrain size in rock salt decreases with increasing differential stress (Carter et al., 1993) and the average subgrain boundary misorientation increases with strain

55 (Pennock et al., 2005). In coarse-grained halite, high finite strain can be accommodated only by formation of subgrains without recrystallization (Linckens et al., 2016). Grain boundary migration can be relatively quick in halite when fluids are present on the grain boundaries (e.g., Schenk & Urai, 2004). In deformation experiments, halite deformed by dislocation creep forms a shape preferred orientation (SPO) and crystallographic preferred orientation (CPO) (e.g., Franssen, 1994; Trimby et al., 2000; Pennock et al., 2005; Zulauf et al., 2010). Field studies indicate that deformation of rock salt in nature often occurs by both

60 processes (e.g., Desbois et al., 2010; Schléder & Urai, 2007).

Although salt formations consist mainly of halite, other evaporite minerals (e.g., calcite/dolomite, anhydrite, carnallite, bischofite,) and impurities (e.g., siliciclastics, clay) occur. For the safety assessment of storage caverns (Yang et al., 2013) and to determine the suitability of the rock salt as geological repository, the mechanical behavior of heterogeneous, impure rock salt needs to be known. Previous research has mainly focused on layered evaporitic sequences, where weak halite or bittern

65 salt (e.g., bischofite, carnallite) layers alternate with stronger anhydrite, mudstone and/or siliciclastic layers (e.g., Hatzor and

Heyman, 1997; Dubey and Gairola, 2008; Rowan et al., 2019; Adamuszek et al., 2021). The range of effective viscosities in these layered evaporitic sequences can be up to five orders of magnitude (Rowan et al., 2019).

The study of folds in a salt mine combined with numerical modelling shows that a small amount (ca. 10%) of impurities (anhydrite and clay) in the rock salt can lead to a viscosity ratio of up to 20 between pure and impure rock salt (Adamuszek et

70 al., 2021). When the strong layers are thicker and form independent mechanical units, they can, depending on the strain geometry, boudinage and form ruptured stringers, or form folds (Rowan et al., 2019).

Small strain (< 10%) deformation experiments have been performed on layered (bedded) rock salt, with thin (mm) layers of impurities (e.g., anhydrite, clay, mud) (Hatzor and Heyman, 1997; Liang et al., 2007; Dubey and Gairola, 2008; Li et al., 2014). These experiments focused on the determination of the elastic parameters, and on the influence of the angle between

75 the bedding and the applied stress on these parameters. In addition, the experiments show the importance of the strong layers on micro-fracture initiation and orientation (Dubey and Gairola, 2008; Li et al., 2014). None of these experiments were succeeded by microstructural investigation of the deformed samples.

Recent cyclic mechanical tests looked at the impact of second-phase content (e.g., anhydrite, clay) on the elastic parameters and deformation processes (Martin-Clave et al., 2021). In these experiments higher second-phase content lead to a weakening

80 due to an increase in the degree of brittle deformation (Martin-Clave et al., 2021). Microstructural analysis shows that the microfracture network in halite was denser in areas with a higher second-phase content (Martin-Clave et al., 2021). A larger amount of clay in the samples also leads to a weakening, which the authors attribute to enhanced pressure solution (Martin-Clave et al., 2021). It has been shown in experiments that pressure solution in halite is promoted at contacts between dissimilar materials likely due to an increase in grain boundary diffusion (Hickman and Evans, 1991; Renard et al., 2001). The increase

85 in pressure solution in "dirty salt" (rock salt with siltstone and dolomite) compared to "clean" rock salt observed in natural deformed samples has also been suggested to lead to the weakening of the dirty salt (Závada et al., 2015).

The previous studies show the importance of impurities (i.e., anhydrite, clay, siliciclastics) on the deformation of rock salt. Previous deformation experiments mainly focused on the elastic parameters and were done to relatively small strains. Furthermore, often microstructural analysis was not conducted. In this paper we present deformation experiments of rock salt

90 with different amounts of siliciclastic material (1 - 53 vol. %). After the experiments we performed a detailed microstructural analysis to determine the deformation mechanisms of the constituent minerals. The siliciclastic domains show brittle deformation, and the halite deforms mainly by dislocation creep accommodated by subgrain formation. In addition, microfractures occur on the halite grain boundaries. The mechanical data suggest that the strength of the rock salt increases with siliciclastic volume fraction. Even when the fraction of siliciclastics is low, there is an influence on the strength, showing

95 the importance of impurities for the deformation of rock salt.

2. Geological setting

For the experiments described in this paper, diapiric Upper Rotliegend (Permian) rock salt of the North German Basin from the salt structure Krempe was used. The structure belongs to the NE-SW trending salt walls of the Glückstadt Graben, situated
100   in the South Permian Basin (SPB, Fig. 1a). Permian deposits form the base of the sedimentary record of the SPB after Permian volcanism and formation of the Central European Basin System. During the Upper Rotliegend, red alluvial, fluvial, playa and salt sediments formed in the SPB before evaporite deposition evolved from continental to full marine during transition from Rotliegend to the Zechstein (Legler et al., 2005; Bachmann et al., 2008, Fig. 1b). The basin center is located in Northern Germany, where continental siliciclastics and evaporites were deposited under arid to semi-arid climates (Glennie, 1987;
105   Stollhofen et al., 2008).

Rotliegend rock salt was mobilized along with marine Zechstein rock salt to form the salt walls of the central Glückstadt Graben with main growth phases during Triassic and Cretaceous extensional events (Maystrenko et al., 2005, 2006). The rock salt fabric typically comprises varying fractions of siliciclastic components as a result of evaporation in a playa setting (Hovorka, 1987; Casas and Lowenstein, 1989), followed by salt fabric reorganization during multiphase deformation
110   (Henneberg et al., 2020).

The material used for experimental deformation is retrieved from the borehole Krempe 1101 drilled in the central part of the salt wall, where Rotliegend rock salt was lifted towards the structural top located at approx. 600 m depth at the drilling site.

3. Deformation apparatus, material and methods

In order to quantify the effect of siliciclastic material on the deformation behavior and the viscosity of rock salt, we carried
115   out thermomechanical experiments on cubes (60 x 60 x 60 mm) from the Rotliegend rock salt under bulk coaxial plane strain (Table 1). The cubes were prepared from the drill cores (100 mm diameter) and the samples have various amount of siliciclastic material (Fig. 2).

Thick sections were prepared from the starting samples using the rock salt adjacent to the samples prepared for deformation (Table 1). In order to show the distribution of siliciclastic material in the samples in three dimensions, CT-scans were made of
120   the samples in the Neuroradiologie Department of Frankfurt University clinic before and after the experiments using a multislice spiral CT-scanner (Phillips Brilliance 6 CT). Conditions for analyzing the samples were as follows: slice thickness (resolution in vertical direction) is 0.4 mm; pixel spacing (resolution in horizontal directions) is 0.07-0.24 mm. From the CT data the approximate volume fraction of siliciclastic material was determined (Table 1). For this purpose, first, the siliciclastic material was selected from the 3D data and displayed separately (Fig. 3). In the following, the sum of the voxels of this data
125   set was determined, and the volume fraction of the total volume was calculated. The error was determined by shrinking or expanding the volume with the resolution in the horizontal directions (0.07-0.24 mm) and in the vertical direction (0.4 mm).

For the deformation experiments we used a specially designed coaxial deformation apparatus, described in detail in Zulauf et al. (2009). In this deformation apparatus the cubes are bounded by plates on four surfaces (Z and Y direction) and can freely

move in the direction of the other two surfaces (*X* direction). To experiments were done at temperatures of 340 °C. To reach

130   this temperature, after loading the sample, the plates are heated up slowly at 10°C/h to 240°C. For the last 100 °C the sample was slowly heated up with 5 °C/h. Some room was left between the sample and the plates, as the samples experience some thermal expansion due to the increase in temperature. The plates were moved slowly after reaching the target temperature, until they touched the surfaces of the cube. The temperature in each plate is monitored by seven thermocouples and kept constant, with an uncertainty less than ± 0.1 °C. Before starting the deformation, the sample was kept overnight, so it was

135   certain that the whole sample reached the high temperatures.

Deformation was started by shortening the cube in the horizontal direction (*Z* direction). To achieve the shortening, the right plate moved towards the left plate. In the vertical direction (*Y* direction) the plates were kept stationary; however, the top plate is pushed to the left by the moving right plate. The sample is not bounded in the *X* direction and extends in that direction (front and back). The deformation is relatively slow, with the right plate moving at a speed of 1mm/day. With a starting length of

140   60mm, using the longitudinal strain (change in length divided by initial length) a shortening strain of 10% is reached after 6 days, which results in a strain rate of ~2 x 10^{-7}. The stress is measured by a point load cell located at the right plate, in the *Z* direction. The load cell can measure stresses up to 4.6 MPa, which defines the stress limits of the deformation experiments. After the target strain is reached (around 20%, when possible), the plate movement is stopped, and the heating is turned off. Comparing the experimental conditions to natural conditions, the main differences are the lack of confining pressure, elevated

145   temperatures and faster strain rates. Natural rock salt can deform at relatively slow strain rates (10^{-16} – 10^{-8} s^{-1}, Talbot ans Jackson, 1987), however the slowest strain is still faster than the strain rate we are using during our experiments ($\dot{e}_Z = 10^{-7}$ s^{-1}). Therefore, and due to the stress limit of 4.6 MPa, the experiments were conducted at elevated temperature (T = 340 °C). Temperatures in natural rock salt and temperatures important for engineering, are in the range of 20-200 °C (Urai et al., 2008). At the deformation conditions listed above, the viscosity of halite is in the range 10^{12} – 10^{13} Pa s (Zulauf et al., 2010, 2011).

150   The viscosity of siliciclastic parts, which largely consist of quartz grains, is several orders of magnitude higher (e.g. Gleason and Tullis, 1995; Rowan et al., 2019), which excludes viscous deformation by dislocation creep.

A thick section is made parallel to the *XZ* plane, in order to avoid boundary effects, the sample was cut at least 1 cm away from the borders. For microstructural analyses, all thick sections were etched for 50 – 60 seconds with a 5.5 molar NaCl-solution and cleaned with n-hexane following the procedure described by Urai et al. (1987) and Zulauf et al. (2010). The thick

155   sections were analyzed with transmitted and reflected optical light microscopy. The subgrain areas were calculated from manually traced subgrain boundaries. The subgrain diameters were determined from the fitted ellipse of equal area using the software ImageJ (https://imagej.nih.gov/ij/). The differential stresses were calculated using the paleopiezometer that is based on the subgrain size of halite (Carter et al., 1993; Schléder and Urai, 2005).

Electron backscatter diffraction (EBSD) measurements of the samples were performed on areas of interest using a JEOL JSM-

160   6490 Scanning Electron Microscope (SEM) with an acceleration voltage of 15 kV and a beam current of ~8 nA. The working distance was between 17 and 20 mm, and the step size was between 3 and 7 µm. Wild spikes were removed, and unindexed pixels were subscribed the average orientation of 6-8 neighbors.

5

4. Results

4.1 Microfabrics of starting material

165 The samples comprise halite with different amounts of fine-grained impurities (Table 1). The volume fractions are an approximation, based on the CT data. In the two samples (GM-HT1 and GM-HT4) with a high amount of detrital material, the detrital domains are heterogeneously distributed (Fig. 2, 3). In the other two samples the detrital grains are dispersed throughout the samples.

The impurities consist of different amounts of anhydrite, quartz, dolomite, feldspar, muscovite-illite, chlorite and hematite.
170 Grain sizes in these detrital domains range between < 20 and 250 µm. Due to their hematite content, most domains show a red to purple color. Halite grains surrounding these domains largely preserve a rounded shape. Halite grain sizes range between 50 µm and 1 cm. Intercrystalline fluid inclusions were observed at halite grain boundaries in all sample specimens (Fig.4 a), while intracrystalline fluid inclusions are lacking.

Areas preserving a high content of detrital grains (GM-HT1), comprise elongated halite forming the infill between detrital
175 domains. Rectangular shaped halite grains are observed also at the contact to detrital domains. Single rectangular shaped halite grains (500 – 2000 µm diameter) are situated within detrital domains.

In areas preserving low content of detrital domains, rounded contacts between halite and detrital domains are observed. Single halite grain boundaries are decorated with small anhydrite crystals or single detrital grains, reaching from detrital domains into the surrounding halite matrix.

180 All samples show subgrains after etching as a result of natural deformation inside the salt structure. In GM-HT1 and GM-HT4 some of these subgrains are elongated (Fig. 4b). Paleodifferential stresses determined from the undeformed samples are in the range of 1.1 – 1.8 MPa, corresponding to average subgrain sizes of 84 – 114 µm (Table 2). Most subgrains have a small misorientation (1-5°, Fig. 5a), although the internal orientation of the grains can be high (up to 15°, Fig. 5b).

185

4.2 Experiments

The experiments show a decrease in stress going from GM-HT1, via GM-HT4, GM-HT2 to GM-HT3 (Fig. 6). This decrease in stress correlates with the volume fraction of siliciclastic material as listed in Table 1. The star in Fig. 6 indicates where the
190 stress was no longer measured accurately in sample GM-HT1 due to the high amount of siliciclastic material. Normally the salt-pressure stamp connection is good because the salt flows, making a tight seal between pressure stamp and rock salt of the sample. However, in sample GM-HT1 the siliciclastic material was in contact with the pressure stamp, leading to inaccurate measurements and significant underestimation of the stress. In addition, after the conditions indicated by the star were obtained,

the deformation stopped as the plates got stuck due to the high strength of the sample. Therefore, the shortening strain of this
sample was limited to only $e_Z = -8\%$.

4.3 Macro- and microstructures of deformed samples

The CT data shows the difference in deformation between the halite dominated rock salt and the siliciclastic domains. The
siliciclastic domains show some brittle deformation with fractures aligned parallel to Z and the opening direction towards X
(Fig. 7b and d). Sometimes fractures occur along the interface between the siliciclastic and the halite domains. The fractures
are open and no salt flowed into these fractures. In contrast to the siliciclastic domains, the halite deforms viscously (ductile)
without fracturing. Some pores are visible within the halite matrix in samples GM-HT2, GM-HT3 and GM-HT4 after
deformation (white arrows, Fig. 7d). In the GM-HT1 sample, the salt extrudes in the X direction in between the siliciclastic
parts (grey arrow, Fig. 7b).

After deformation, the halite grains of samples GM-HT2, GM-HT3 and GM-HT4 are elongated in the X direction (average
grain aspect ratio of 3.6 in GM-HT2, Fig. 8). Halite displays additional subgrains as a result of the deformation experiments.
Subgrains are preserved in all areas of the analyzed thick sections (Fig. 8), with the exception of halite grains enclosed in large
detrital domains of sample GM-HT1, where only few subgrain boundaries are visible (Fig. 9b). The average subgrain sizes are
smaller (19 - 39 µm) compared to the subgrains of the initial samples. The average subgrain size has a large standard deviation
due to large variation in subgrain sizes in some grains (Fig. 9a and c). Subgrain sizes correspond to average differential stresses
between 4.4 MPa (GM-HT2) and 8.2 MPa (GM-HT1) (Table 2).

Many grains in samples GM-HT2 and GM-HT3, and a few in sample GM-HT4, contain bands with aligned small subgrains
surrounded by larger subgrain domains (Fig. 9a and c). Throughout all investigated areas of experimentally deformed samples,
fluid inclusions are present along grain boundaries similar to those of the starting samples (Fig. 9d). The subgrain boundaries
mainly show small misorientations (1-5°), but there are segments with larger misorientations (5-10°, Fig. 10a). There are also,
in some grains, longer parallel segments of newly formed grain boundaries (misorientation >10°, Fig. 10b).

The EBSD data shows that the grains with the small aligned subgrains splits up into alternating bands with a similar orientation
(Fig. 11a). Even though many of the small subgrains show a small misorientation (1-5°), the bands can have a misorientation
exceeding 20° (Fig. 11b).

5. Discussion

5.1. Mechanical data and microfabrics

The stress-strain curves show the dependence of the stress in halite on the amount of siliciclastic material. Even a small amount
of siliciclastic material (GM-HT3, ~1%) increases the stress in halite (Fig. 6). In contrast to previous experiments on anhydrite-
halite samples (Martin-Clave et al., 2021) and studies on natural rock salt (Závada et al., 2015) the stress increases with

increasing second-phase content. An increase in stress has also been observed in naturally deformed samples, with smaller subgrains in halite close to anhydrite particles (Mertineit et al., 2014; Thiemeyer et al., 2016). The weakening in the other studies was due to an enhancement of pressure solution resulting from increased diffusion on the halite-solid phase interfaces. The microfabrics of samples of the present study shows that the deformation of halite was mainly taken up by grain boundary fractures (Fig. 7) and dislocation creep accommodated by subgrain formation (Figs. 8-11). In the experimentally deformed samples the subgrains do not rotate enough to form new grains, and the grain size remains large (Fig. 8). The subgrains do sometimes form bands where the boundaries of the bands form new high-angle grain boundaries. This lack of new grains and the formation of aligned subgrain bands with high-angle boundaries at the borders has been previously observed in deformation experiments on pure rock salt samples (Linckens et al., 2016, 2019).

The formation of small subgrains at the border of the bands and larger ones within the bands (Fig. 9c) leads to a large range of subgrain sizes (Table 2). Therefore, even though the measured stresses for sample GM-HT2 and GM-HT3 are much lower than the calculated stresses (Fig. 6), they are within error. The high stresses calculated for sample GM-HT1 show that the stresses were likely much higher than recorded. This is due to inaccurate stress measurements; the siliciclastic material was in contact with the pressure stamp, prohibiting the required link between the pressure stamp and rock salt (siliciclastic material does not flow during the experiment). Moreover, the differential stress within the halite of one and the same sample may be inhomogeneous depending on the distance of the halite grain to the siliciclastic part. When approaching rigid phases, such as anhydrite or siliciclastic material, the stress in viscously deforming halite can increase significantly. A decrease in subgrain size in the vicinity of anhydrite, due to increase in stress, has been observed for naturally (Mertineit et al., 2014; Thiemeyer et al., 2016) and experimentally deformed samples (Zulauf et al., 2011) and can be explained by increasing amounts of dislocations in halite at the contact to the rigid phases. However, in these experiments no decrease in subgrain size has been observed in the vicinity of the siliciclastic domains.

In the samples with a small amount of siliciclastic material (GM-HT2 and GM-HT3), the grains are elongated in the *X* direction, which in combination with the newly formed subgrain boundaries indicates dislocation creep as dominant deformation mechanism. It is likely that due to the large grain size, pressure solution was less important as deformation mechanism in these samples. During the deformation experiments on anhydrite-halite composite samples (Liang et al., 2007), the composite samples have mechanical properties between the end member lithologies. No weakening was observed in these composite samples due to the anhydrite. This is similar to the results of our experiments; however no microstructural analysis was performed after their experiments (Liang et al., 2007).

They also observe that with increasing confining pressure the difference in mechanical properties between the end member lithologies and composite samples decrease. A composite flow law where the viscosity of a two-phase rock depends on the volume fraction of the two phases and the end-member flow laws has been developed (e.g., Ji et al., 2003). In order to test this model for our samples, we need more data (i.e., the end member flow law of siliciclastics and halite-siliciclastic samples with a higher volume fraction of siliciclastics). However, in these models the strength of the composite increases even when only a small volume fraction of a stronger phase is added (Ji et al., 2003). This is in contrast to the model of the "interconnected weak

layer (IWL)", where the rheology of the composite can be described by the weakest phase in the rock, when this phase is

260   interconnected (Handy, 1994). Even though in samples GM-HT2 and GM-HT4 the halite is interconnected (Fig. 2), the strength

of these samples is larger than that of sample GM-HT3 with less amount of siliciclastics (Fig. 6). The results of our experiments

are more in accordance with the composite flow model. In order to model the viscosity of these composite rock salt samples,

it is important to consider the siliciclastic phase, even when the volume fraction is small (< 10 vol.%).

5.2. Deformation mechanisms

265   It is clear from the CT data that even though most deformation is taken up by the much weaker halite in the samples with small

amounts of siliciclastic material (GM-HT2 and GM-HT3), some of the siliciclastic material shows brittle deformation (Fig.

7d). The fractures in the siliciclastic material in all samples are subparallel to Y and Z and open in the X direction (Fig. 7). A

few fractures occur at the interface between the rock salt and the siliciclastic domains. Very thin layers of halite within the

siliciclastic parts, which are oriented subperpendicular to the least principal stress (σ_3), may have acted as breaking planes (Fig.

270   7b). In most cases, the rock salt does not fill the new fractures during the experiment. Similar observations have been made

during thermomechanical experiments of rock salt/anhydrite interbeddings, which have been carried out under pure

constriction, plane strain and pure flattening (Zulauf et al., 2009, 2010, 2011, 2012; Mertineit et al., 2012). These experiments

were carried out under similar conditions like those used during the present study. Due to high finite strain, the anhydrite layers

were boudinaged and the halite was able to flow into the necks between the boudins. Most of the necks were entirely filled

275   with halite, but some remained partly open.

In addition to the larger fractures, the halite often shows microfractures along the grain boundaries (Fig. 8). The importance of

impurities on the fracturing has been studied in previous experiments (e.g., Dubey & Gairola, 2008; Li et al., 2014; Martin-

Clave et al., 2021). The study of (Martin-Clave et al., 2021) shows that microcracks in halite occur in areas with a high fraction

of second phases (e.g., anhydrite, polyhalite). In our experiments there is not a direct link between the halite grain boundary

280   fractures and siliciclastic content. Our experiments were performed without a confining pressure (in contrast to the experiments

of (Martin-Clave et al., 2021). It would be interesting to see what microfractures and fractures remain when the experiments

are conducted under a confining pressure. It is likely that many of the grain boundary microfractures in halite disappear (Peach

et al., 2001), whereas the fractures in the siliciclastic domains remain. In addition to the fractures, some pores within halite can

be seen on the CT images of sample GM-HT1, GM-HT2 and GM-HT3 (arrows in Fig. 7d) after deformation. Most of these

285   pores are not related to the siliciclastic domains, and thus are difficult to explain.

5.3. Importance of the new results for engineering and applied projects

The present experiments have been carried out under largely dry conditions. In nature, the open fractures in siliciclastic parts

may form pathways for migrating fluids, which are not desired in host rocks of a waste repository. In cases that the siliciclastic

parts are entirely enclosed by viscous halite, the fractures will not contribute to long-distance fluid migration. However, if the

290   siliciclastic parts are interconnected over a large vertical distance, the fractures may form a pervasive fluid network, which

could imply dispersion of radionuclides or of other hazardous material from deeper structural levels up to the biogenic zone. Moreover, fluids within the siliciclastic parts would have a significant impact on the deformation mechanisms of halite: (1) As rock salt is acting as a seal, the fluid pressure may increase supporting continuous brittle deformation by hydrofracturing (Secor, 1965). (2) The fluids will enhance pressure solution and related deformation by solution-precipitation creep (Rutter,

295   1976, 1983). Solution precipitation creep is common in halite because of its high solubility (Spiers et al., 1990; Hickman and Evans, 1991) and is particularly effective when halite is mixed with clay or other phases (Bos and Spiers, 2001; Renard et al., 2001). However, solution-precipitation creep of rock salt is restricted to open natural systems, which are common in salt rocks situated close to the surface or in salt glaciers. Salt rocks of these environments are affected by brittle behavior and dilatancy, which support pathways for migrating fluids (e.g., Talbot et al., 2000; Talbot and Aftabi, 2004; Desbois et al., 2010;

300   Adamuszek et al., 2021). At deeper structural levels, brittle deformation and dilatancy are less frequent. Newly formed open fractures will be closed by the higher confining pressure and by self-sealing of rock salt due to its flow by dislocation creep and precipitation of salt minerals from brine.

6. Conclusions

- Increasing amounts of siliciclastics in rock salt result in increasing differential stress of the matrix halite.
305 - Although most of the finite strain was accommodated by the viscous halite, and stresses in the latter were not homogenous, the flow of halite was largely controlled by subgrain formation without significant recrystallization.
- Thin layers of halite within siliciclastic parts of salt rocks may act as breaking planes if aligned subperpendicular to the least principal stress (σ_3).
- Siliciclastic parts within rock salt are forming brittle domains at upper structural levels, which may deform by
310 fracturing. The barrier behavior of such rocks is significantly reduced, particularly in cases where the siliciclastic parts and their fractures are interconnected making pervasive ascendant fluid transport possible.
- Future thermomechanical experiments of impure rock salt should be carried out with the application of confining pressure, which should have a significant impact on the opening of brittle fractures.

Author contribution

Competing interests

320 The authors declare that they have no conflict of interest.

References

Adamuszek, M., Tămaş, D. M., Barabasch, J., and Urai, J. L.: Rheological stratification in impure rock salt during long-term creep: Morphology, microstructure, and numerical models of multilayer folds in the Ocnele Mari salt mine, Romania, Solid Earth, 12, 2041–2065, https://doi.org/10.5194/se-12-2041-2021, 2021.

330 Bachmann, G. H., Voigt, T., Bayer, U., von Eynatten, H., Legler, B., and Littke, R.: Depositional history and sedimentary cycles in the Central European Basin System, in: Dynamics of complex intracontinental basins. The Central European basin system, edited by: Littke, R., Bayer, U., Gajewski, D., and Nelskamp, S., Springer, Heidelberg, 181–210, 2008.

Baldschuhn, R., Binot, F., Frisch, U., and Kockel, F.: Geotektonischer Atlas von Nordwest-Deutschland und dem deutschen Nordsee-Sektor, Geologisches Jahrbuch, vol. v. A 153, 88 pp. pp., 2001.

335 von Berlepsch, T. and Haverkamp, B.: Salt as a host rock for the geological repository for nuclear waste, 12, 257–262, 2016.

Bornemann, O., Behlau, J., Fischbeck, R., Hammer, J., Jaritz, W., Keller, S., Mingerzahn, G., and Schramm, M.: Description of the Gorleben Site Part 3. Results of the geological surface and underground exploration of the salt formation, BRG, Hannover, 223 pp., 2008.

Bos, B. and Spiers, C. J.: Experimental investigation into the microstructural and mechanical evolution of phyllosilicate-
340 bearing fault rock under conditions favouring pressure solution, J. Struct. Geol., 23, 1187–1202, https://doi.org/10.1016/S0191-8141(00)00184-X, 2001.

Carter, N. L. and Hansen, F. D.: Creep of rocksalt, Tectonophysics, 92, 275–333, 1983.

Carter, N. L., Horseman, S. T., Russell, J. E., and Handin, J.: Rheology of rocksalt, J. Struct. Geol., 15, 1257–1271, 1993.

Casas, E. and Lowenstein, T. K.: Diagenesis of saline pan halite; comparison of petrographic features of modern, Quaternary
345 and Permian halites, J. Sediment. Res., 59, 724–739, https://doi.org/doi: https://doi.org/10.1306/212F905C-2B24-11D7-8648000102C1865D, 1989.

Desbois, G., Závada, P., Schléder, Z., and Urai, J. L.: Deformation and recrystallization mechanisms in actively extruding salt fountain: Microstructural evidence for a switch in deformation mechanisms with increased availability of meteoric water and decreased grain size (Qum Kuh, central Iran), J. Struct. Geol., 32, 580–594, https://doi.org/10.1016/j.jsg.2010.03.005, 2010.

350 Desbois, G., Urai, J. L., and de Bresser, J. H. P.: Fluid distribution in grain boundaries of natural fine-grained rock salt deformed at low differential stress (Qom Kuh salt fountain, central Iran): Implications for rheology and transport properties, J. Struct. Geol., 43, 128–143, https://doi.org/10.1016/j.jsg.2012.07.002, 2012.

Deutsche Stratigraphische Kommission (2016): Stratigraphische Tabelle von Deutschland 2016. http://www.stratigraphie.de/std/index.html

355 Dubey, R. K. and Gairola, V. K.: Influence of structural anisotropy on creep of rocksalt from Simla Himalaya, India: An experimental approach, J. Struct. Geol., 30, 710–718, https://doi.org/10.1016/j.jsg.2008.01.007, 2008.

Franssen, R. C. M..: The rheology of synthetic rocksalt in uniaxial compression, Tectonophysics 233, 1–40, 1994.

Gast, R. E., Dusar, M., Breitkreuz, C., Gaupp, R., Schneider, J. W., Stemmerik, J. W., Geluk, M. C., Geissler, M., Kiersnowski, H., Glennie, K. W., Kabel, S., and Jones, N. .: Rotliegend, in: Petroleum Geological Atlas of the Southern Permian Basin Area,

360 edited by: Dornenbaal, J. C., Stevenson, A. G., EAGE Publications b.v. (Houten), 101–121, 2010.

Glennie, K. W.: Desert sedimentary environments, present and past—A summary, Sediment. Geol., 50, 135–165, 1987.

Handy, M.: Flow laws for rocks containing two non-linear viscous phases: a phenomenological approach, J. Struct. Geol., 16, 287–301, 1994.

Hatzor, Y. H. and Heyman, E. P.: Dilation of anisotropic rock salt: Evidence from Mount Sedom diapir, J. Geophys. Res., 102,

365 14,814-853,868, 1997.

Ter Heege, J. H., De Bresser, J. H. P., and Spiers, C. J.: Rheological behaviour of synthetic rocksalt: the interplay between water, dynamic recrystallization and deformation mechanisms, J. Struct. Geol., 27, 948–963, https://doi.org/10.1016/j.jsg.2005.04.008, 2005.

Henneberg, M., Linckens, J., Schramm, M., Hammer, J., Gerdes, A., and Zulauf, G.: Structural evolution of continental and

370 marine Permian rock salt of the North German Basin: constraints from microfabrics, geochemistry and U–Pb ages, Int. J. Earth Sci., 109, 2369–2387, https://doi.org/10.1007/s00531-020-01905-w, 2020.

Hickman, S. H. and Evans, B.: Experimental pressure solution in halite: the effect of grain/interphase boundary structure, J. Geol. Soc. London, 148, 549–560, 1991.

Hovorka, S.: Depositional environments of marine-dominated bedded halite, Permian San Andres Formation, Texas.,

375 Sedimentology, 34, 1029–1054, 1987.

Hubbert, M. K.: Theory of scale models as applied to the study of geologic structures, Bull. Geol. Soc. Am., 48, 1459–1520, 1937.

Hudec, M. R. and Jackson, M. P. A.: Terra infirma: Understanding salt tectonics, Earth-Science Rev., 82, 1–28, https://doi.org/10.1016/j.earscirev.2007.01.001, 2007.

380 Ji, S., Zhao, P., and Xia, B.: Flow laws of multiphase materials and rocks from end-member flow laws, Tectonophysics, 370, 129–145, https://doi.org/10.1016/S0040-1951(03)00182-3, 2003.

Kneuker, T., Zulauf, G., Mertineit, M., Behlau, J., and Hammer, J.: The impact of finite strain on deformation mechanisms of Permian Stassfurt rock salt at the Morsleben site (Germany): constraints from microfabric studies and EBSD analyses, Zeitschrift der Dtsch. Gesellschaft für Geowissenschaften, 165, 91–106, https://doi.org/10.1127/1860-1804/2013/0041, 2014.

385 Küster, Y., Leiss, B., and Schramm, M.: Structural characteristics of the halite fabric type 'Kristallbrocken' from the Zechstein Basin with regard to its development, Int. J. Earth Sci., 99, 505–526, https://doi.org/10.1007/s00531-008-0399-8, 2008.

Legler, B., Gebhardt, U., and Schneider, J. W.: Late Permian non-marine-marine transitional profiles in the central Southern Permian Basin, northern Germany, Int. J. Earth Sci., 94, 851–862, https://doi.org/10.1007/s00531-005-0002-5, 2005.

Li, Y., Liu, W., Yang, C., and Daemen, J. J. K.: Experimental investigation of mechanical behavior of bedded rock salt
390 containing inclined interlayer, Int. J. Rock Mech. Min. Sci., 69, 39–49, https://doi.org/10.1016/j.ijrmms.2014.03.006, 2014.

Liang, W., Yang, C., Zhao, Y., Dusseault, M. B., and Liu, J.: Experimental investigation of mechanical properties of bedded salt rock, Int. J. Rock Mech. Min. Sci., 44, 400–411, https://doi.org/10.1016/j.ijrmms.2006.09.007, 2007.

Linckens, J., Zulauf, G., and Hammer, J.: Experimental deformation of coarse-grained rock salt to high strain, J. Geophys. Res. Solid Earth, 2010, 6150–6171, https://doi.org/10.1002/2016JB013070.Received, 2016.

395 Linckens, J., Zulauf, G., and Mertineit, M.: The influence of a grain-shape fabric on the mechanical behaviour of rock salt: Results from deformation experiments, Tectonophysics, 751, 73–82, 2019.

Martin-Clave, C., Ougier-Simonin, A., and Vandeginste, V.: Impact of Second Phase Content on Rock Salt Rheological Behavior Under Cyclic Mechanical Conditions, Rock Mech. Rock Eng., 54, 5245–5267, https://doi.org/10.1007/s00603-021-02449-4, 2021.

400 Maystrenko, Y., Bayer, U., and Scheck-Wenderoth, M.: Structure and evolution of the Glueckstadt Graben due to salt movements, Int. J. Earth Sci., 94, 799–814, https://doi.org/10.1007/s00531-005-0003-4, 2005.

Maystrenko, Y., Bayer, U., and Scheck-Wenderoth, M.: 3D reconstruction of salt movements within the deepest post-Permian structure of the Central European Basin System - The Glueckstadt Graben, Geol. en Mijnbouw/Netherlands J. Geosci., 85, 181–196, https://doi.org/10.1017/S0016774600021466, 2006.

405 Mertineit, M., Behlau, J., Hammer, J., Schramm, M., and Zulauf, G.: Mechanical behavior of anhydrite rocks: results of field investigations, mineralogical-geochemical studies and thermomechanical experiments.itle, in: Mechanical behavior of salt VII: Proceedings of the 7th Conference, edited by: Bérest, P., Ghoreychi, M., Hadj-Hassen, F., and Tijani, M., Taylor & Francis Group, London, 123–129, 2012.

Mertineit, M., Schramm, M., Hammer, J., Zulauf, G., and Mertineit, M.: Deformation of anhydrite rocks (Gorleben-Bank,
410 z3OSM) in a high-strain domain of the Gorleben salt dome, Germany, Zeitschrift der Dtsch. Gesellschaft für Geowissenschaften, https://doi.org/10.1127/1860-1804/2013/0048, 2014.

Peach, C. J., Spiers, C. J., and Trimby, P. W.: Effect of confining pressure on dilatation, recrystallization, and flow of rock salt at 150°C, J. Geophys. Res., 106, 13315–13328, 2001.

Pennock, G. M., Drury, M. R., and Spiers, C. J.: The development of subgrain misorientations with strain in dry synthetic

415 NaCl measured using EBSD, J. Struct. Geol., 27, 2159–2170, https://doi.org/10.1016/j.jsg.2005.06.013, 2005.

Peryt, T. M., Geluk, M. C., Mathiesen, A., Paul, J., and Smith, K.: Zechstein, in: Petroleum Geological Atlas of the South Permian Basin Area, EAGE Publications bv Houten, 123–147, 2010.

Ramberg, H.: Gravity, Deformation and the Earth´s Crust, Academic Press, London, 452 pp., 1981.

Renard, F., Dysthe, D., Feder, J., Bjorlykke, K., and Jamtveit, B.: Enhanced pressure solution creep rates induced by clay

420 particles ' Experimental evidence in salt aggregates, Geophys. Res. Lett., 28, 1295–1298, 2001.

Rowan, M. G., Urai, J. L., Carl Fiduk, J., and Kukla, P. A.: Deformation of intrasalt competent layers in different modes of salt tectonics, Solid Earth, 10, 987–1013, https://doi.org/10.5194/se-10-987-2019, 2019.

Rutter, E. H.: A discussion on natural strain and geological structure-the kinetics of rock deformation by pressure solution, Philos. Trans. R. Soc. London. Ser. A, Math. Phys. Sci., 283, 203–219, 1976.

425 Rutter, E. H.: Pressure solution in nature, theory and experiment., J. Geol. Soc. London., 140, 725–740, https://doi.org/10.1144/gsjgs.140.5.0725, 1983.

Schenk, O. O. and Urai, J. L.: Microstructural evolution and grain boundary structure during static recrystallization in synthetic polycrystals of sodium chloride containing saturated brine, Contrib. to Mineral. Petrol., 146, 671–682, https://doi.org/10.1007/s00410-003-0522-6, 2004.

430 Schléder, Z. and Urai, J. L.: Microstructural evolution of deformation-modified primary halite from the Middle Triassic Röt Formation at Hengelo, The Netherlands, Int. J. Earth Sci., 94, 941–955, https://doi.org/10.1007/s00531-005-0503-2, 2005.

Schléder, Z. and Urai, J. L.: Deformation and recrystallization mechanisms in mylonitic shear zones in naturally deformed extrusive Eocene–Oligocene rocksalt from Eyvanekey plateau and Garmsar hills (central Iran), J. Struct. Geol., 29, 241–255, https://doi.org/10.1016/j.jsg.2006.08.014, 2007.

435 Secor, D. T.: Role of fluid pressure in jointing, Am. J. Sci., 263, 633–646, 1965.

Skrotzki, W., Dornbusch, H.-J., Helming, K., Tamm, R., and Brockmeier, H.-G.: Development of microstructure and texture in pure shear deformed salt, in: The Mechanical Behaviour of Salt: Proceedings of the Fourth Conference Series on Rock and Soil Mechanics, edited by: Aubertin, M. and Hardy, H. R., TTP Trans Tech Publications, Clausthal-Zellerfeld, 101–114, 1996.

Spiers, C. J. and Urai, J. L.: The effect of grain boundary water on deformation mechanisms and rheology of rocksalt during

440 long-term deformation, in: The Mechanical Behaviour of Salt – Understanding of THMC Processes in Salt, edited by: M, W. and Lux KH, Minkley W, H. H. J., Taylor & Francis Group, London, 149–58, 2007.

Spiers, C. J., Schutjens, P. M. T. M., Brzesowsky, R. H., Peach, C. J., Liezenberg, J. L., and J., Zwart, J. H.: Experimental determination of constitutive parameters governing creep of rocksalt by pressure solution, Geol. Soc. London, Spec. Publ., 54, 215–227, 1990.

445 Staudtmeister, K. and Rokahr, R. B.: Rock mechanical design of storage caverns for natural gas in rock salt mass, Int. J. Rock Mech. Min. Sci., 34, paper No. 300, 1997.

Stollhofen, H., Bachmann, G., Barnasch, J., Bayer, U., Beutler, G., Franz, M., Kaestner, M., Legler, B., Mutterlose, J., and Radies, D.: Upper Rotliegend to Early Cretaceous Basin Development, Dyn. Complex Intracont. Basins, 181–210, 2008.

Talbot, C. J. and Aftabi, P.: Geology and models of salt extrusion at Qum Kuh, central Iran, J. Geol. Soc. London., 161, 321–
450   334, https://doi.org/10.1144/0016-764903-102, 2004.

Talbot, C. J. and Jackson, M. P. A.: Internal kinematics of salt diapirs, Am. Assoc. Pet. Geol. Bull., 71, 1068–1093, 1987.

Talbot, C. J., Medvedev, S., Alavi, M., Shahrivar, H., and Heidari, E.: Salt extrusion at Kuh-e-Jahani, Iran, from June 1994 to November 1997, Geol. Soc. Spec. Publ., 174, 93–110, https://doi.org/10.1144/GSL.SP.1999.174.01.06, 2000.

Thiemeyer, N., Zulauf, G., Mertineit, M., Linckens, J., Pusch, M., and Hammer, J.: Microfabrics and 3D grain shape of
455   Gorleben rock salt: Constraints on deformation mechanisms and paleodifferential stress, Tectonophysics 676, 1–19, https://doi.org/10.1016/j.tecto.2016.02.046, 2016.

Trimby, P. W., Drury, M. R., and Spiers, C. J.: Recognising the crystallographic signature of recrystallisation processes in deformed rocks: a study of experimentally deformed rocksalt, J. Struct. Geol., 22, 1609–1620, 2000.

Urai, J. L., Spiers, C. J., Zwart, H. J., and Lister, G. S.: Weakening of rock salt by water during long-term creep, Nature, 324,
460   554–557, 1986.

Urai, J. L., Schléder, Z., Spiers, C. J., and Kukla, P. A.: Flow and Transport Properties of Salt Rocks, in: Dynamics of Complex Intracontinental Basins: The Central European Basin System, edited by: Littke, R., Bayer, U., Gajewski, D., and Nelskamp, S., Springer-Verlag Berlin, Heidelberg, 277–290, 2008.

Yang, C., Jing, W., Daemen, J. J. K., Zhang, G., and Du, C.: Analysis of major risks associated with hydrocarbon storage
465   caverns in bedded salt rock, Reliab. Eng. Syst. Saf., 113, 94–111, https://doi.org/10.1016/j.ress.2012.12.017, 2013.

Závada, P., Desbois, G., Urai, J. L., Schulmann, K., Rahmati, M., Lexa, O., and Wollenberg, U.: Impact of solid second phases on deformation mechanisms of naturally deformed salt rocks (Kuh-e-Namak, Dashti, Iran) and rheological stratification of the Hormuz Salt Formation, J. Struct. Geol., 74, 117–144, https://doi.org/10.1016/j.jsg.2015.02.009, 2015.

Zulauf, G., Zulauf, J., Bornemann, O., Kihm, N., Peinl, M., and Zanella, F.: Experimental deformation of a single-layer
470   anhydrite in halite matrix under bulk constriction. Part 1: Geometric and kinematic aspects, J. Struct. Geol., 31, 460–474, https://doi.org/10.1016/j.jsg.2009.01.013, 2009.

Zulauf, G., Zulauf, J., Bornemann, O., Brenker, F. E., Höfer, H. E., Peinl, M., and Woodland, A. B.: Experimental deformation of a single-layer anhydrite in halite matrix under bulk constriction. Part 2: Deformation mechanisms and the role of fluids, J. Struct. Geol., 32, 264–277, https://doi.org/10.1016/j.jsg.2009.12.001, 2010.

475   Zulauf, G., Zulauf, J., Mertineit, M., and Hammer, J.: Boudinage of anhydrite in rock-salt matrix: The impact of bulk finite strain geometry, in: Mechanical behavior of salt VII: Proceedings of the 7th Conference, edited by: Bérest, P., Ghoreychi, M., Hadj-Hassen, F., and Tijani, M., Taylor & Francis Group, London, 65–70, 2012.

Zulauf, J., Zulauf, G., Hammer, J., and Zanella, F.: Tablet boudinage of an anhydrite layer in rock-salt matrix: Results from thermomechanical experiments, J. Struct. Geol., 33, 1801–1815, https://doi.org/10.1016/j.jsg.2011.09.006, 2011.

480
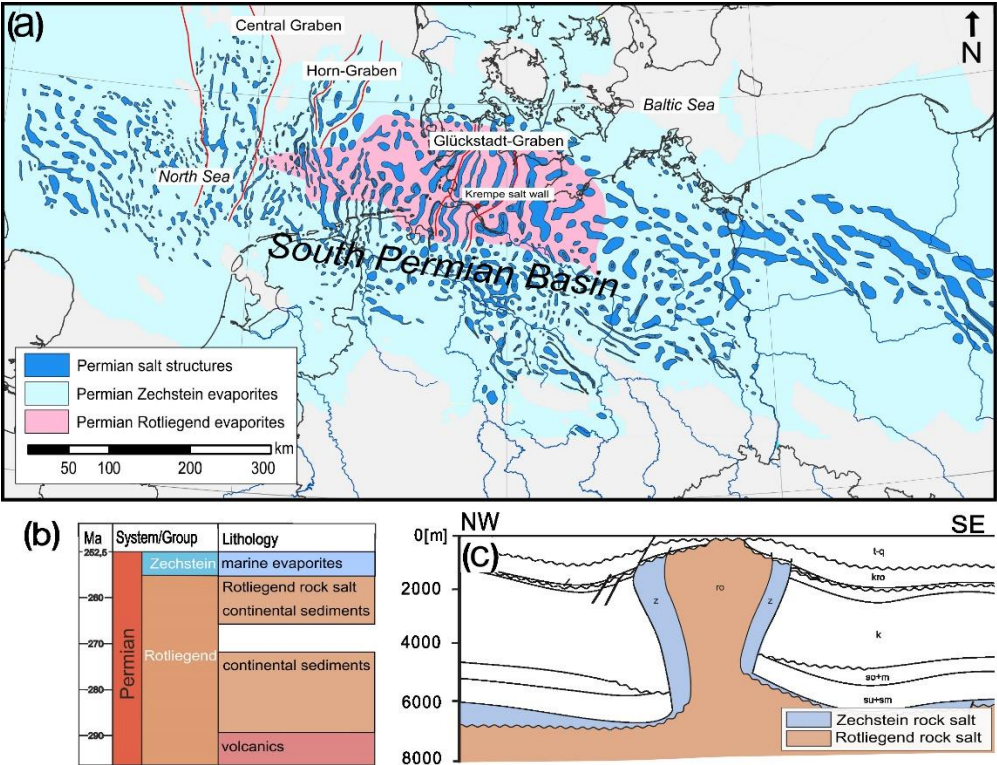
Figure 1: a) Location of the Krempe salt wall within the SPB (after Maystrenko et al., 2005; Gast et al., 2010; Peryt et al., 2010). b) Lithostratigraphy of Permian deposits of northern Germany (after DSK, 2016). c) Distribution of Permian rock salt in a cross section of the Krempe salt wall (after Baldschuhn et al., 2001).
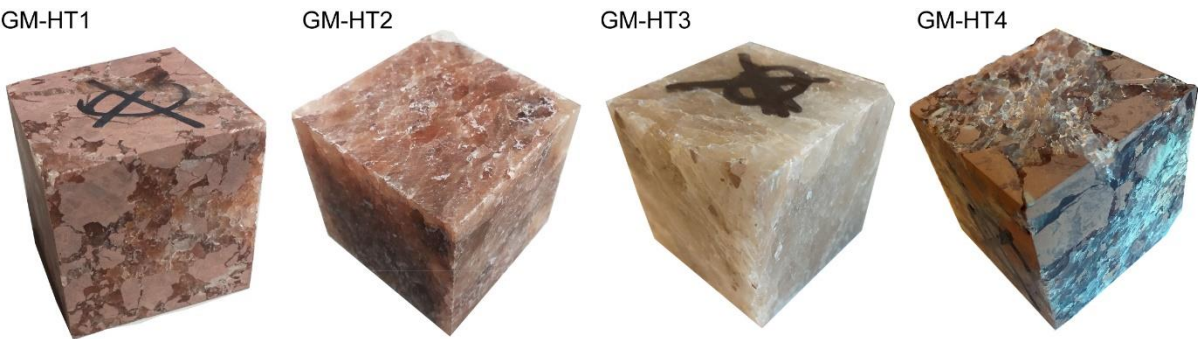

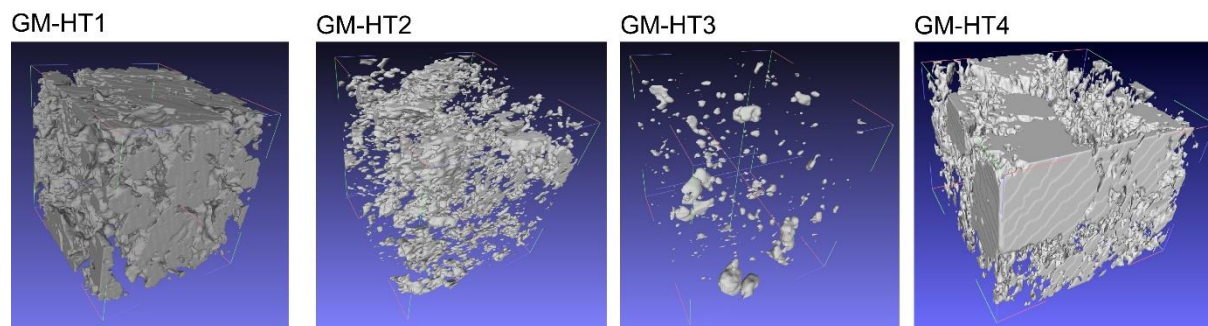Figure 2: The four cubes of rock salt (60x60x60 mm) before experimental deformation.

Figure 3: Distribution of the siliciclastic material in the four initial cubes (60x60x60 mm) derived from the CT data. Rock salt of the matrix is omitted.

495
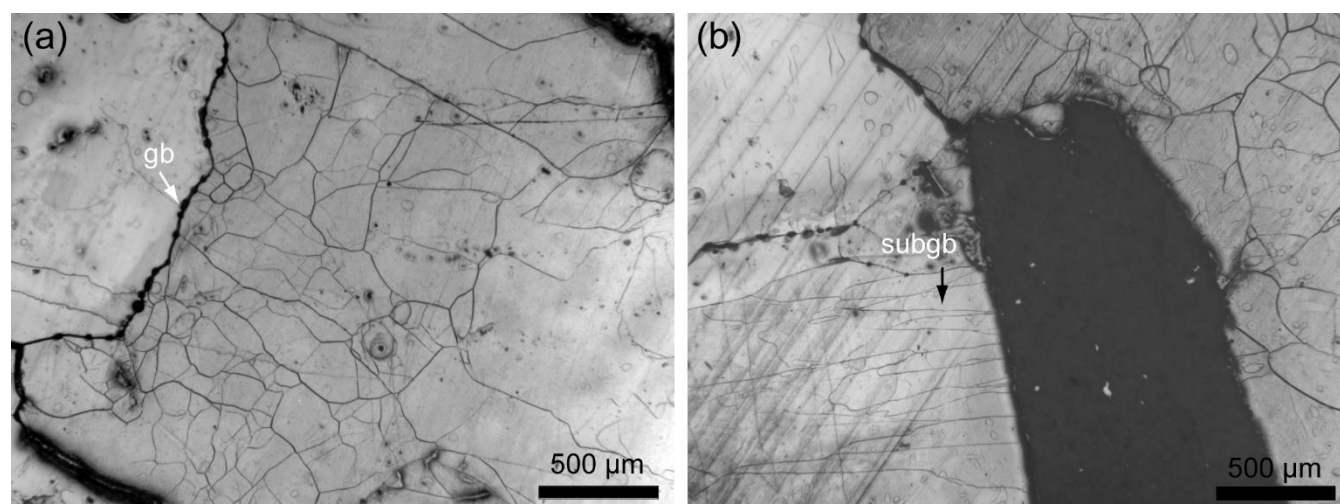
Figure 4: Optical microscope reflected light images of the starting microstructures. a) One halite grain with no subgrains (left) and one with subgrains (right). Fluid inclusions are located on the grain boundary (white arrow). b) Halite grains and a detrital grain (black). The halite grain on the left shows elongated subgrains (black arrow). Subvertical scratches result from the preparation and etching procedure.
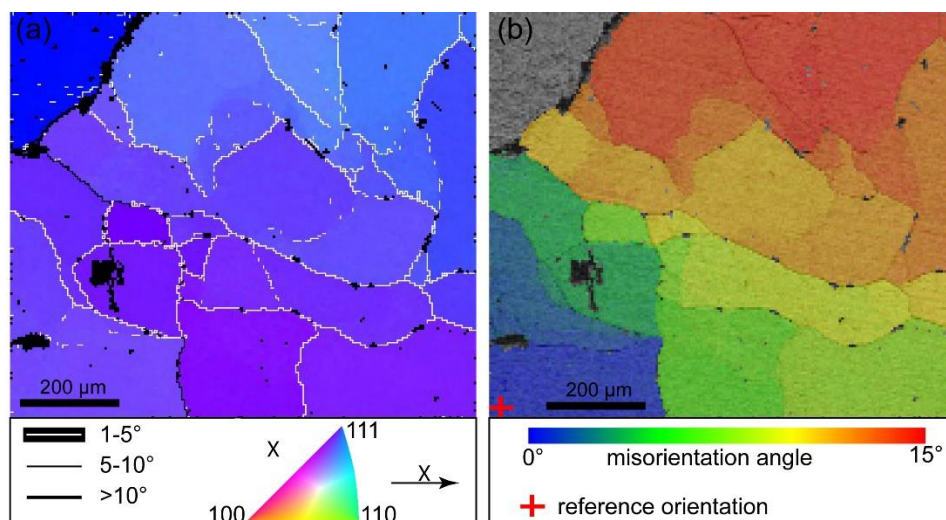
500

17

Figure 5: EBSD data of halite of initial sample. a) IPF colour map of halite orientations showing subgrains. b) Misorientation data for the halite grain. The internal misorientation goes up to 15° in a distance of about 700 μm.
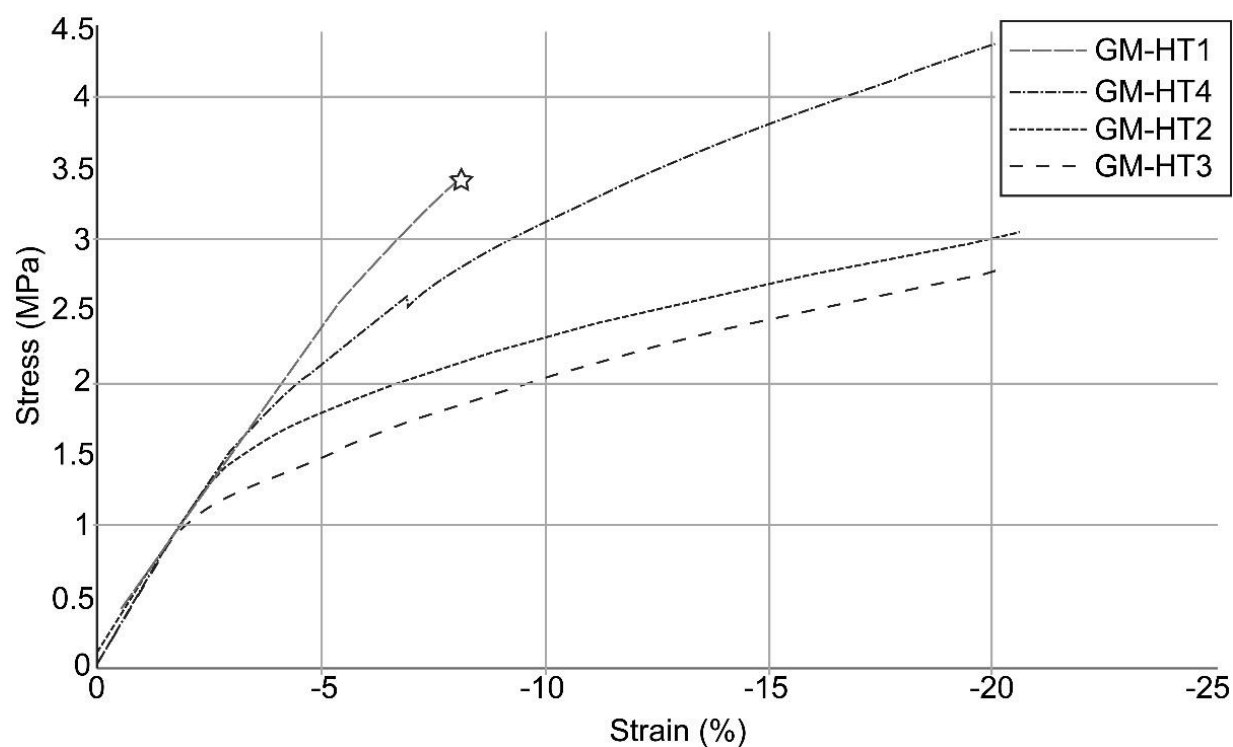

505

Figure 6: Strain (e_Z) vs. stress (σ_Z) graph of the four samples.
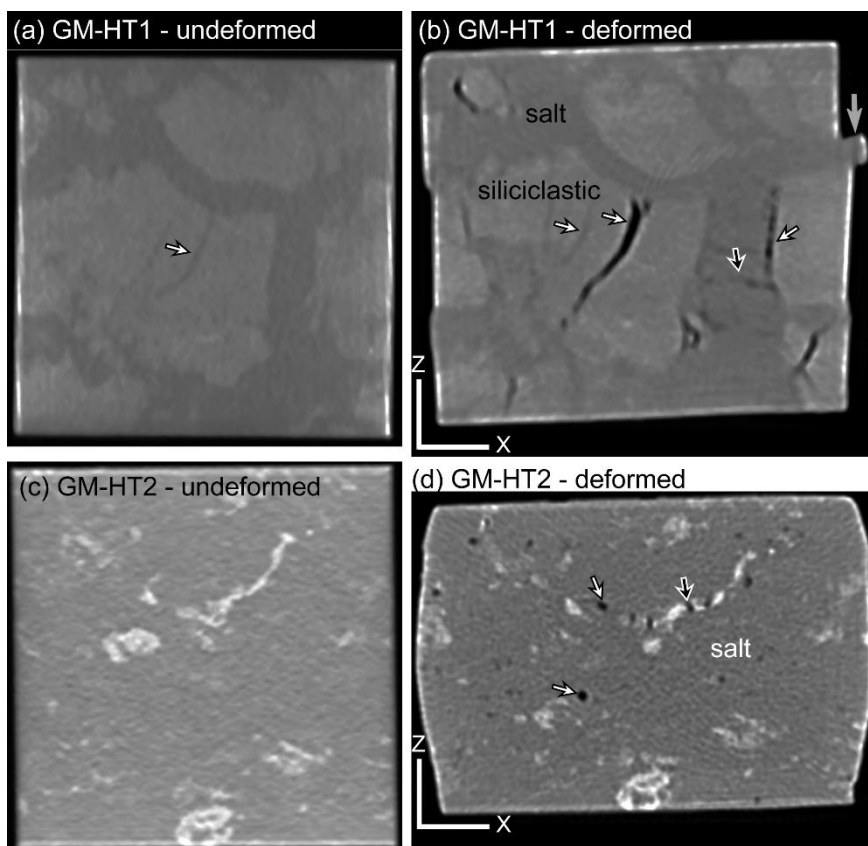
Fig. 7. Selected CT images of two samples GM-HT1 and GM-HT2. a) CT image of the undeformed sample GM-HT1. Thin layers of salt (dark grey) are separating the siliciclastic material (light grey). There are some very fine lines of halite in between the siliciclastic material (arrow). b) CT image of sample GM-HT1 (location similar to a.) after experimental deformation. There are some vertical fractures (//Z, arrows). The salt extrudes in the X direction (grey arrow). There seems to be a horizontal fracture in the salt (black arrow). c) CT image of undeformed sample GM-HT2 showing a few small areas of siliciclastic material (white) within the rock salt matrix (dark grey). d) CT image of experimentally deformed sample GM-HT2 showing fractures parallel to Z (black arrow) and some round pores (white arrow).
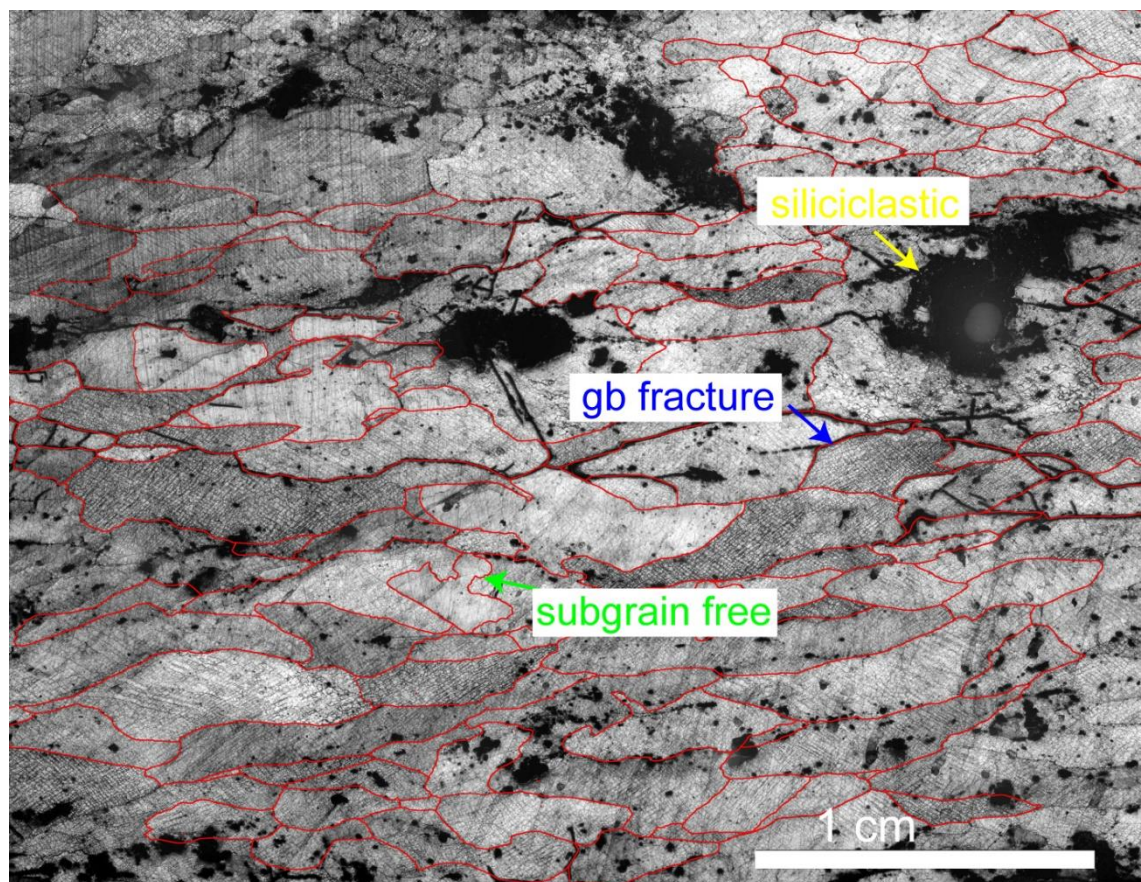
19

Figure 8: Reflected light microscopic overview of experimentally deformed sample GM-HT2 (XZ section). The grain boundaries are traced in red. The dark domains are siliciclastic (yellow arrow). There are some grain boundary fractures (blue arrow). Most grains show subgrains and some of them are aligned in one direction. There are a few grains with no subgrains (green arrow).
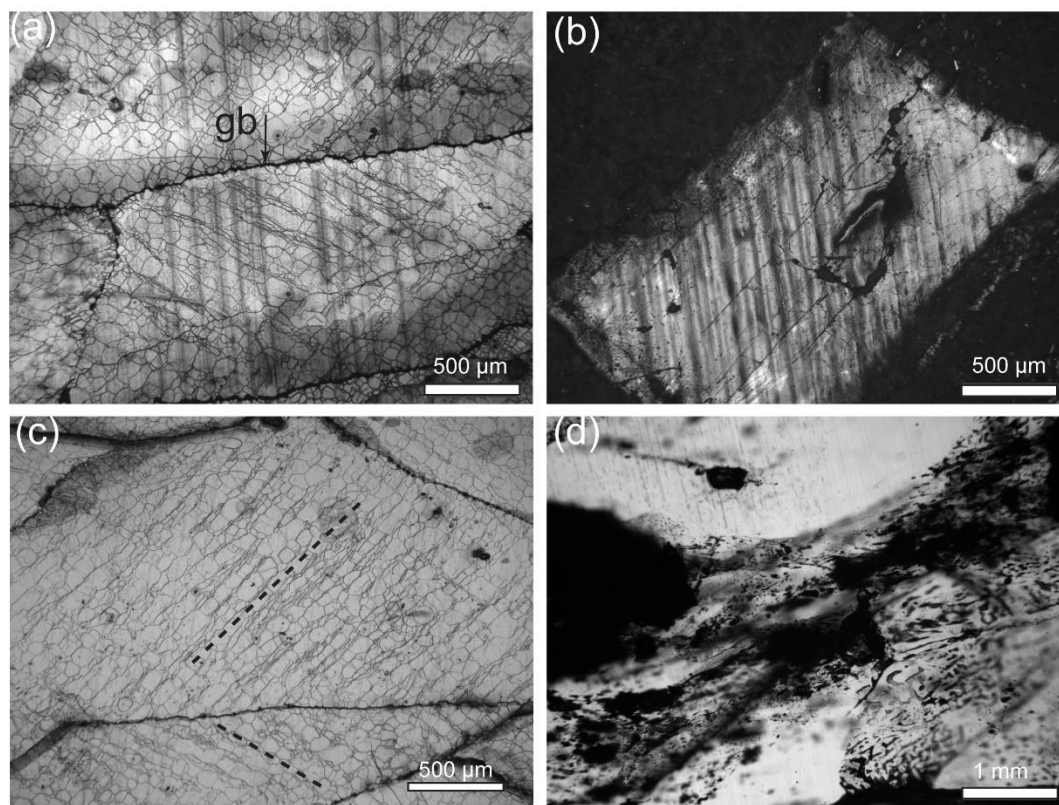
530

535

540

Figure 9: Reflected light microscopic images (a-c) and transmitted light image (d) of experimentally deformed samples. a) Subgrains in sample GM-HT2. Both grains show subgrains. The lower grain shows aligned subgrains in bands, with very small subgrains. b) Halite grain enclosed in siliciclastic domain (black) in sample GM-HT2 shows no subgrains. c) Subgrain bands in sample GM-HT3. d) Fluid inclusions on halite grain boundaries in sample GM-HT2. Vertical scratches in (a) and (b) result from the preparation and
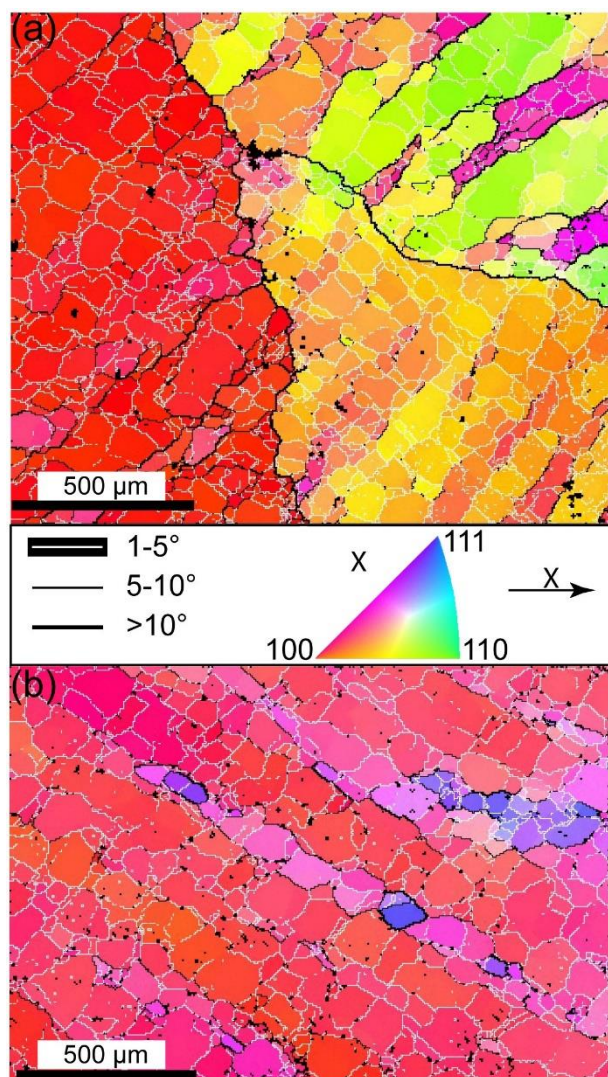545 **etching procedure.**

Figure 10: Inverse pole figure orientation maps of experimentally deformed sample GM-HT1 (a) and GM-HT2 (b). a) shows three halite grains with subgrains. Most subgrains have a misorientation between 1 and 5°, however two grains show the formation of segments of new grain boundaries (>10°). These are oriented in one direction, and do not enclose an area. b) One halite grain showing subgrains with mainly 1-5° misorientation and some small segments which are >10°.

550

555
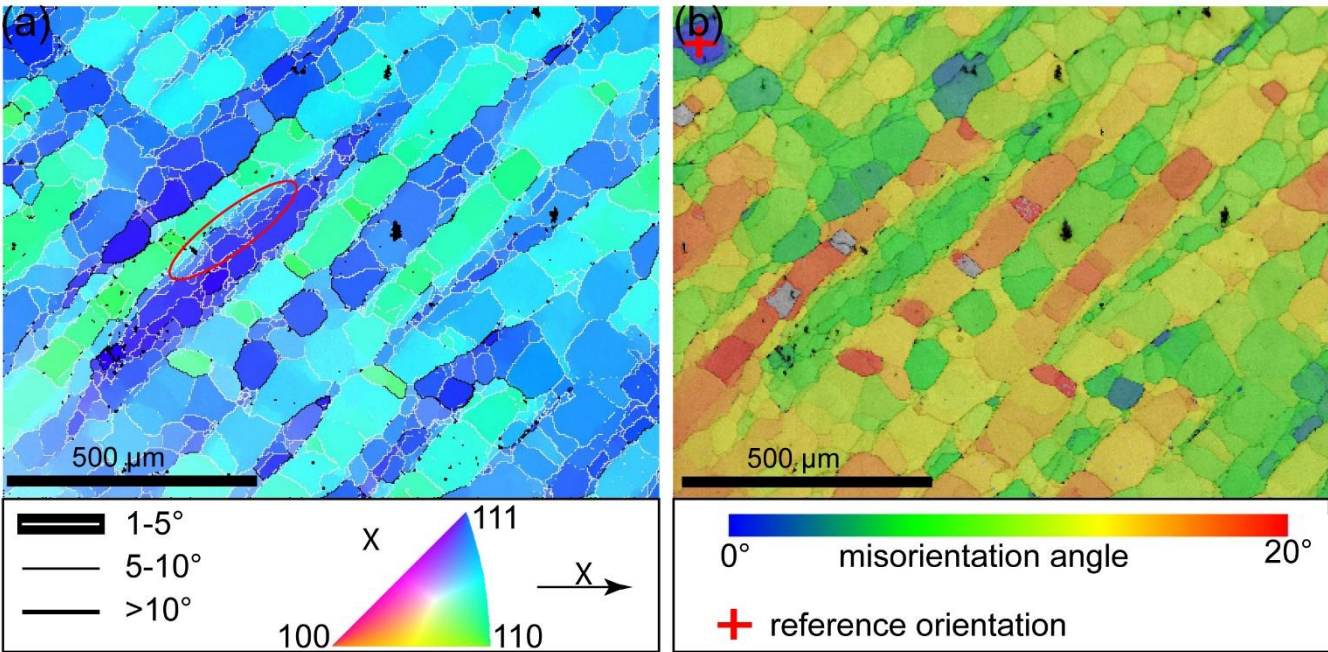
Figure 11: EBSD data of sample GM-HT3 after experimental deformation. a) IPF orientation map of halite showing alternating bands with different orientations and small subgrains (red circle). Some border segments of the bands have a high misorientation (>10°). b) Deviation in misorientation angle map from the reference orientation going up to 20°. The map shows the high misorientation within the grain (>20°), even though there are not many newly formed grain boundaries. There are some grey grains within the high misorientation angle bands that have misorientations >20°.

Table 1. Sample borehole depths and approximate volume fraction of siliciclastic material.

experimentally deformed samples		starting samples		
sample name	depth [m]	sample name	depth [m]	volume fraction siliciclastic
GM-HT1	666.50 – 666.24	GM1-ND	666.2 – 666.24	0.53 ± 0.06
GM-HT2	724.59 – 724.65	GM3-ND	724.76 – 724.8	0.07 ± 0.02
GM-HT3	1234.48 – 1234.55	GM-HT3-ND	1234.49 – 1234.53	0.008 ± 0.003
GM-HT4	1274.92 – 1275.00	GM6-ND	1273.18 – 1273.22	0.38 ± 0.06

Table 2: Calculated (paleo-)stresses (σ_{diff}) of starting and experimentally deformed samples based on size of subgrains (d_{sub}).

Experimentally deformed samples				
sample	d_{sub} [µm]	*st. dev*. [µm]	σ_{diff} [Mpa]	No. of analyzed subgrains
GM-HT1	19	12	8.2	2449
GM-HT2	39	27	4.4	1295

GM-HT3	35	31	4.8	1357
GM-HT4	35	29	4.8	1122
starting samples				570
sample	d_{sub} [µm]	*st. dev.* [µm]	σ_{diff} [Mpa]	No. of analyzed Subgrains
GM1-ND	152	84	1.3	612
GM3-ND	154	94	1.3	584
GM-HT3-ND	110	96	1.8	642
GM6-ND	190	114	1.1	521

575

580

24